Toolbox for *in vivo* imaging of host-parasite interactions at multiple scales

Mariana De Niz*[1,2#], Florentin Spadin*[3], Matthias Marti[2], Jens V. Stein[4,5], Martin Frenz[3], Friedrich Frischknecht[6]

[1] Institute of Cell Biology-Heussler lab, University of Bern, Switzerland
[2] Wellcome Centre for Molecular Parasitology, University of Glasgow, UK
[3] Institute of Applied Physics, University of Bern, Switzerland
[4] Theodor Kocher Institute, University of Bern, Switzerland
[5] Department of Oncology, Microbiology and Immunology, University of Fribourg, Switzerland
[6] Integrative Parasitology, Centre for Infectious Diseases, Heidelberg University Medical School, Germany

Current affiliation: Instituto de Medicina Molecular – João Lobo Antunes, Faculdade de Medicina, Universidade de Lisboa, Portugal
*Authors equally contributed

Correspondence
Mariana De Niz, Instituto de Medicina Molecular – João Lobo Antunes, Faculdade de Medicina, Universidade de Lisboa, Portugal
Email: mariana.deniz@medicina.ulisboa.pt

Abstract

Animal models have for long been pivotal for parasitology research. Over the last few years, techniques such as intravital, optoacoustic and magnetic resonance imaging, optical projection tomography, and selective plane illumination microscopy developed promising potential for gaining insights into host-pathogen interactions by allowing different visualization forms *in vivo* and *ex vivo*. Advances including increased resolution, penetration depth, and acquisition speed, together with more complex image analysis methods facilitate tackling biological problems previously impossible to study and/or quantify. Here we discuss advances and challenges in the *in vivo* imaging toolbox, which hold important potential for the field of parasitology.

Keywords

Parasitology, imaging, *in vivo*, animal models

Imaging toolbox in parasitology

Imaging techniques developed for biomedical applications have had an important impact in parasitology research. Such techniques include platforms developed to image host-pathogen interactions at various scales, ranging from molecules to whole organisms (summarised in **table 1**). These techniques have complementary advantages with respect to each other. This review focuses on the technological advances used for visualization of host-pathogen interactions either *in vivo,* or *ex vivo* in whole organisms in five imaging techniques: intravital microscopy (IVM), optical projection tomography (OPT), bioluminescence imaging, optoacoustic imaging (OAI), and magnetic resonance imaging (MRI).

Advanced fluorescence methods applied to intravital microscopy

Intravital microscopy (IVM) is a powerful technique to investigate dynamic cellular processes and host-parasite interactions within functioning organs. Organs studied by IVM in the context of parasitology include the brain [1–4], the skin [5–7], the placenta [8,9], the lungs [10], the liver [11–13], and the spleen [14,15] (summarized in **table 2,** green=IVM exists; yellow=organ relevant but IVM never done; grey = IVM not done). Important advances in parasitology have been achieved using wide-field epifluorescence, confocal, spinning disc, or two-photon IVM. Recent developments, which have expanded the applications of IVM include the generation of

longer wavelength excitation lasers; a wider range of fluorescent reporters for dyes; transgenic fluorescence reporter mice and parasites; fluorescence lifetime measurements; adaptive optics; imaging windows and micro-endoscopes, but also software advances for high throughput automated analyses and motion correction. Moreover, for fixed specimens, tissue-clearing techniques providing deeper optical penetration into organs have opened new avenues of research [16].

Longer wavelength excitation lasers offer substantial advantages for IVM. Wavelengths in the 700-1000 nm excitation range are to some extent limited by penetration depth and background emission from tissue endogenous signals. Ultrafast tuneable infrared lasers are now available which enable imaging at 1300 nm overcoming both problems [17]. Longer wavelength light is less scattered and absorbed by tissues, as long as the wavelength is shorter than the water absorption peaks, resulting in deeper optical penetration. This new generation of lasers, coupled with novel far-red probes take advantage of wavelengths that elicit less autofluorescence signals, thus helping to improve the signal-to-noise ratio. Moreover, phototoxicity to tissues is believed to be reduced at longer wavelengths [18]. Further, wavelength mixing of synchronized lasers, or multi-photon excitation achieved either via dual output laser sources, or specialized lasers such as the recently reported femtosecond diamond Raman laser [19], enable multi-colour imaging, expanding the range of structures that can be studied *in vivo* by IVM. In parallel, a wide range of fluorescent probes in the form of immuno-fluorophores, genetic tags, quantum dots, and organic dyes have been developed over the past few years to study dynamic processes *in vivo* including protein-protein interactions, and host-pathogen interactions in healthy and diseased states (Reviewed in [20,21]).

Microscopy tools that are key to investigate cell or protein dynamics and interactions *in vitro*, have in recent years successfully permeated into IVM (Reviewed in [22]). Examples of these methods include Förster resonance energy transfer (FRET), fluorescence loss in photobleaching (FLIP), and fluorescence recovery after photobleaching (FRAP). FRET in mice has been achieved by either of two methods: the generation of transgenic animals with chromophores acting as partners for resonance energy transfer, or the transfection of cells followed by their transfer into living animals [23]. FRET poses important challenges in IVM, which are usually not encountered in *in vitro* conditions. These include signal strength limitations, photobleaching and photodamage. Initially, FRET was mostly used as a ratiometric technique in IVM, allowing the measurement of relative changes of different parameters of interest at high speed, generally using the fluorescent proteins cerulean and citrine as donor and acceptor fluorophores, respectively. Despite the value of ratiometric FRET, one of its main limitations is its dependence on relative quantifications rather

than absolute measurements. So far, FRET has not been reported *in vivo* in parasitology, yet could be very useful to monitor the activity of kinases, proteases, GTPases [24]; calcium changes [25]; lipid concentrations [23,26–28] during infection; and even physical stresses such as temperature, mechanical stressors, or electromagnetic fields [29], as well as molecular interactions between host and pathogens; host cell subsets, or parasite molecules. Likewise, there has been significant progress in the development of software to allow separate quantification of signals from single cells in complex 3D environments, such as those present in organs of living animals [30,31].

Another set of fluorescence methods increasingly adapted to IVM are FRAP and FLIP. Both techniques are generally used to monitor molecular movement within cells, and are amenable to repeated use *in vivo* without causing tissue damage. They are particularly useful to assess macromolecular flux across cells and tissues. Both methods yield information such as half-time to recovery, rate of movement of fluorescent molecules within and between cellular compartments, and molecular transfer between regions independent of rate of movement. Like FRET, FRAP and FLIP have been largely explored in 2D environments using cell cultures, but have only recently been incorporated into *in vivo* research [22]. This has been possible due to the generation of transgenic mice with fluorescent reporters expressed in specific cell types, cell-cell junctions, or other structures. Particularly useful for the study of parasite cell migration, invasion and development, would be reporter mice that enable quantification of dynamic regulation of cell-cell junctions (e.g. E-cadherin-GFP) [32], or studying micro-vessel leakiness as a proxy of endothelial barrier function using dyes such as FITC-Dextran or albumin [33].

Super-resolution microscopy has gained significant momentum for use in *in vitro* imaging over the past decade, and its application in IVM contexts brings about equally exciting prospects. One limitation that prevented its faster adaptation to IVM, is the light scattering which results in depth-dependent deterioration of spatial resolution, due to spherical aberrations to the point spread function in complex tissue [34]. Although not yet used in the field of parasitology, other fields have developed methods to achieve super resolution microscopy while imaging living animals. Examples include a recently developed setup which incorporates multi-beam striped illumination, spatial modulation of excitation, and laser scanning microscopy [35], or the use of STED to achieve super-resolution to observe morphological changes of actin in the brain [36].

In addition to microscopy methods applicable to IVM, the use of optical windows and micro-endoscopes has greatly benefited various research fields, including parasitology, to enable long term imaging of organs throughout multiple days (reviewed in [37]). While most optical

windows are limited to the surface of the surgically exposed organs, GRIN lenses and micro-endoscopes enable access to deeper regions [38], otherwise inaccessible, including deeper structures in the brain, the spinal cord, the bone marrow, the lungs and the heart [38–41]. Both micro-endoscopes and temporary optical windows have benefited imaging parasites, giving insights into phenomena including parasite crossing of endothelial barriers enabling relevant to their dissemination across tissues, dynamics relevant to parasite survival, and mechanisms of transmission to and from the insect vectors. Further progress for penetration depth and resolution in living samples, has been achieved by adaptive optics, which is widely applied in astronomy. Biological specimens have refractive-index inhomogeneities which affect resolution. Adaptive optics allows reversing signal/resolution degradation by pre-distorting the wavefront of the incoming light to cancel distortions occurring in the light path [42].

Finally, a significant challenge for IVM is motion induced by breathing, peristalsis, and circulation, which mostly affects organs in the chest and abdomen. A significant achievement for image analysis in IVM is automation for motion artefact removal [43,44]. This includes triggering imaging at specific time periods to coincide with the heartbeat or respiration or triggering heart contractions to coincide with image acquisition. Conversely, various pieces of software have been generated for image analysis, which allow correction of sample motion following image acquisition [45]. These methods are applicable to different laser scanning modalities, including confocal and multi-photon microscopy.

Optical projection tomography (OPT) and selective plane illumination microscopy (SPIM)

Photon scattering in tissues hinders imaging at depths exceeding a few hundred micrometers *in vivo*, making imaging of whole organs impossible. Hence, imaging at depth requires the physical sectioning of tissues due to photon scattering. The imaging limit of conventional microscopy in terms of penetration depth is set by a physical parameter of photons known as the mean free path (MFP) (reviewed in [46]). The MFP translates as the number of scattering or collision events that a photon undergoes, each of which modifies the photon's direction of travel, ultimately resulting in image blur. For widefield epifluorescence microscopy a traditional thickness for tissue sections is 10-50 μm, which ensures high image quality, and diffraction-limited resolution. Confocal and multi-photon microscopy allow greater penetration depths of up to 0.5 to 1 mm. Nevertheless, to acquire a 3D image of an entire sample using confocal or multi-photon

microscopy, automated methods for the digital reconstruction of thin serial sections require acquisition of hundreds of individual sections and/or long imaging periods under high energy illumination. This ultimately renders confocal and multi-photon techniques impractical for imaging intact, large specimens.

Mesoscopic imaging techniques such as light sheet fluorescence microscopy (LSFM; also called selective plane illumination microscopy: SPIM) and optical projection tomography (OPT) enable visualization of larger fields of view across entire organs. The prerequisite is that these organs must be transparent or optically cleared. Tissue clearance has gained significant momentum in recent years, as shown by a rising number of clearing methods which offer different advantages, despite their use being limited to fixed tissues [47–49]. Altogether, tissue clearance methods must satisfy three basic criteria: a) all tissues must be efficiently cleared, b) cellular and sub-cellular structures must be adequately preserved, and c) tissue clearance must be compatible with fluorescence detection. Current techniques include the use of organic solvents [50–53], water [47,54,55], and electrophoresis-based protocols [56,57]. A summary of relevant methods for tissue clearance is shown in **table 3.**

Once the sample is transparent, OPT imaging is achieved via tissue trans- and epi-illumination over multiple projections [58]. With the OPT setup, the specimen is rotated through 360 degrees in angular steps around a single axis while being held in position for imaging **(Figure 1a)**. Virtual sections are independently reconstructed from the acquired images using a back-projection algorithm [59]. This method allows high resolution imaging at penetration depths of up to 15 millimeters [58]. As a result, high resolution digital sections, and 3D image reconstructions of the sampled specimen's volume can be obtained.

LSFM in contrast, uses a thin plane of light (or light sheet), that is shaped by a cylindrical lens or a laser scanner to exclusively illuminate the focal plane of the sample at any one time and has been used extensively to image living, if small organisms (**Figure 1b**) [60]. While in conventional microscopes illumination and detection follows the same path, the detection pathway in LSFM is rotated by 90°. Altogether, these characteristics make it a powerful tool for live cell imaging of large samples due to its high imaging speed, reduced toxicity, and photobleaching (reviewed by [61]). 3D image formation is based on raw images being assembled after translation or rotation of the entire sample. Multiple LSFM setups have been developed, including illumination from multiple directions which enable doubling the penetration depth [62], or combining different mesoscopic techniques, including OPTiSPIM (Optical projection

tomography integrated in light sheet microscopy) [63], a hybrid setup which benefits from the high resolution of SPIM with the possibility to image fluorescent and non-fluorescent contrasts of OPT. The first commercial devices were made available and an open source, custom built-version named OpenSPIM was produced [64,65]. OPT and/or LSFM have been used to image multi-cellular culture models [66–69], zebrafish [70], sparse cell populations [71], the development of plants [72], living embryos and gene mapping [58,73], as well as multiple rodent organs in health and disease conditions [50,53,74,75]. OPT and LSFM were both successfully used to obtain detailed insight of the anatomy of the flight musculature of a *Drosophila* fly, its nervous and digestive systems, and ß-galactoside activity at whole-body level [76,77]. While in its origins, the application of tissue clearing and imaging was limited to rodent organs or small whole bodies (such as that of *Drosophila* flies), a build up on previous hydrogel embedding, tissue clearing techniques (PACT), imaging reagents (RIMS), and delivery routes (PARS) made it possible to image whole optically cleared mice [78].

In parasitology, uses have included the generation of optically cleared guts from Tsetse flies (vectors of *Trypanosoma brucei*) [79] (**Figure 1c**) and optically transparent *Anopheles* mosquitoes (vectors of *Plasmodium*) (**Figure 1d-1e**). Importantly, the use of mesoscopic methods in parasitology has remained scarce, despite their relatively easy implementation and use. The potential of these techniques to study interactions at high resolution, and high throughput for the phenotypic characterization of parasite-induced changes in vectors, rodents, and other model organisms is high, and worth exploring and implementing in various areas of parasitology in years to come.

Bioluminescence imaging

Photon production is achieved primarily through luminescence and fluorescence. Both processes yield photons as a consequence of energy transitions from excited-state molecular orbitals to lower energy orbitals. However, they differ in how the excited state orbitals are created. In luminescence, the excited state is the product of exothermic chemical reactions, whereas in fluorescence the excited states are created by absorption of light. The main advantage of luminescence assays is accurate quantification with high sensitivity, which can be applied in high throughput studies, both *in vivo* and *in vitro*. Luminescence is generated through a chemical reaction where the enzyme (e.g. luciferase) oxidizes a substrate (e.g. luciferin), leading to photon emission.

Bioluminescence imaging relies on processes occurring in nature via the generation of light

by lower organisms including beetles, bacteria, mollusks, algae, crustaceans, annelids and coelenterates [80]. Various bioluminescent substrates have been isolated from these organisms, and their biochemical properties have been defined (**Figure 2**). Across parasitology research, the main bioluminescent probe used *in vivo* is firefly luciferase (reviewed by [81,82]), with *Gaussia*, NanoLuc and *Renilla* luciferase being less commonly used. Transgenic *Plasmodium spp., Toxoplasma spp., Leishmania spp., Trypanosoma brucei,* and *Trypanosoma cruzi* expressing bioluminescent probes have been used for investigating parasite growth and dissemination, virulence, co-infections, parasite stage-specific promoters, drug-screening, and monitoring host-pathogen interactions (reviewed by [81,82]).

In recent years, an important aim has been to achieve ultra-bright luminescence to detect signals with high sensitivity in deep tissues. This has been initially achieved by generating parasites expressing codon-optimized red-shifted firefly luciferases [83,84] and ultra-bright luminescent probes such as NanoLuc [85,86]. Although NanoLuc luciferase has been extremely useful *in vitro* due to the extremely bright signal it produces [87], its performance *in vivo* is very poor due to its short emission wavelength. Recently, a novel red-shifted luciferase-luciferin pair based on the coelenterazine analogue diphenylterazine (DTZ) and a NanoLuc mutant fused to a fluorescent reporter (resulting in a ultra-bright probe known as Antares2), proved to be highly successful for *in vivo* imaging [88,89]. Similarly, another highly successful combination has been that of AkaLumine hydrochloride (AkaLumine-HCl- a synthetic D-luciferin analogue), which when catalysed by Firefly luciferase generates near-infrared emission, and has favourable distribution in deep organs [90]. Random mutagenesis of firefly luciferase-based libraries led to the generation of Akaluc, which displayed high thermostability and the brightest emission when combined with AkaLumine [91]. The AkaLuc/AkaLumine-HCl combination has allowed a revolutionary advance, namely visualization of single bioluminescent cells in deep tissues of freely moving animals [91].

Further technological advances in the field of bioluminescence include dual-probe reporters which allow detecting two signals simultaneously, at different wavelengths. These have been useful in the context of characterization of different promoters expressed at different parasite life stages [92,93]. Equally, bioluminescence can be used in the context of bioluminescence energy transfer (BRET), or hybrid biosensors (BRET-FRET, or hyBRET) for investigation of protein-protein interactions, analysis of xenografts, and optogenetics, *in vivo* [94].

Optoacoustic imaging and ultrasound

All optical imaging techniques mentioned above have been shown to image biological structures with subcellular resolution (in the range of the wavelength used) and remarkable contrast but are limited by strong light scattering in tissue. Optoacoustic (OA) imaging, also referred to as photoacoustic imaging, offers the ability to not only overcome this limitation but to provide structural, functional, metabolic and even molecular information [95,96]. OA is a hybrid imaging modality, combining optics and acoustics via the thermoelastic effect [97,98]. The thermoelastic effect converts optically absorbed energy into acoustic waves, which are recorded at the tissue surface by means of ultrasound detection. Optical absorption provides the imaging contrast for OA, which means that any chromophore or molecule that selectively absorbs the illumination wavelength can be imaged [99]. Chromophores can be endogenous, such as haemoglobin, which provide via their spectral fingerprint quantitative and physiological information of the vasculature, or exogenous, such as antibodies functionalized by absorbing metallic nanoparticles or dyes suited to the assessment of tumours and other pathologies. These features make OA imaging an interesting technique for studying host-parasite interactions.

Imaging can be performed both in a tomographic macroscopic setup visualizing the whole animal or in a microscopic setup. Tomography uses an array of ultrasound sensors, often partially or completely surrounding the target, to achieve image resolution of typically a few hundred micrometers, determined by the bandwidth of the ultrasound transducer and imaging depths of up to few centimetres [100]. In contrast, microscopy setups use a single mechanically scanned focused transducer (**Figure 3a**) or a tightly focused diffraction limited laser beam to generate an image. In the former case, termed acoustic resolution microscopy, the resolution is given by the properties of the acoustic lens and the ultrasound transducer (~40 μm at 50 MHz transducer frequency). In this configuration, OA microscopy has been shown to resolve fine structures in the dermis and assess dermal papillae [101]. It has also been used to visualize the cerebral vascular anatomy in mice up to a depth of 3.7 mm at submillimeter resolution (sub-100 μm at 1 mm depth), greatly surpassing what can be achieved with purely optical techniques [102]. In the latter case, called optical resolution microscopy, the lateral resolution is determined by the focal spot of the laser and imaging depth is limited by optical scattering to maximum of 1 mm, as it is in the case of pure optical microscopy [100,103]. In low-scattering tissue such as that found in mouse ears, the resolution can be pushed to 2.5 μm at a depth of 150 μm [104].

Both contrast and penetration depth are affected by the choice of excitation wavelength. Shorter wavelengths (typically no shorter than 532 nm) are strongly absorbed by haemoglobin and thus higher contrast can be achieved, at the expense of penetration depth. For longer wavelengths (typically up to 1300 nm), penetration depth is increased at the expense of contrast. Since the

propagation speed of ultrasound waves in biological tissue is comparatively low, depth information can be obtained by recording the pressure wave in a time-resolved manner. Thus, all OA imaging techniques have the potential to obtain three-dimensional images. Furthermore, differences in the wavelength-dependent absorption coefficients of oxygenated and deoxygenated haemoglobin can be utilised for oxygenation measurements in both tomographic [105] and microscopic setups [102,104].

Currently, only a few commercially available *in vivo* whole animal OA imaging devices are capable of capturing single cross-sectional tomographic images of living small animals with estimated in-plane resolutions of ~ 150 μm [106–108]. OA tomography has also been combined with echo-ultrasound imaging in a whole-body live mouse tomography system, with reported in-plane spatial resolutions of 150 μm (OA) and 350 μm (ultrasound) [109].

Using acoustic resolution OA microscopy (**Figure 3a**), we have imaged the brain of mice aged 4 - 6 weeks infected with *Plasmodium*. The mice had their scalp removed (the skull was left intact) prior to imaging and were kept under anaesthesia during imaging. We have found that images of healthy mice (**Figure 3b**) show clearly discernible hemispheres and cerebellum, while in infected mice (5 days after infection) the major vascular landmarks could hardly be identified. The vasculature showed a large number of chaotically distributed screw-like blood vessels and the two hemispheres could no longer be distinguished (**Figure 3c**). In later stages of the disease (7+ days after infection), a significant decrease in optoacoustic signal amplitude was detected, possibly due to progressive anaemia.

Altogether, OA imaging, which combines high contrast and spectral sensitivity with the high spatial resolution obtained in ultrasound imaging, provides excellent visualization of microvasculature, making it a powerful tool for basic parasitological research and pre-clinical applications. Combined with exogenous optically absorbing agents or genetically expressed reporters it has been proven to provide molecular information with high sensitivity and specificity.

While OA imaging is a hybrid technique employing ultrasound as one of its components, ultrasound imaging itself has also been successfully used in the field of parasitology and in medical imaging. Ultrasound uses high-frequency sound waves, which are reflected off of body structures, rendering an image. Key advances in ultrasound over the past decade include elastography [110], ultrasound contrast agent imaging using micro-bubbles (reviewed by [111]), super resolution imaging, 2D array transducer, and ultra-fast ultrasound imaging [112]. While these advances have been widely explored in other fields of research, they remain to be used in *in vivo* parasitology, and have enormous potential. Elastography is a technique referred to as "palpating by imaging",

enabling measurement and visualization of tissue mechanical properties in health and disease. In terms of contrast agents, microbubbles provide considerable advantages to ultrasound imaging, including the possibility of studying blood rheology and tissue perfusion, and of enhancing vascular permeability, drug and gene delivery, and local heating (reviewed by [113]). Finally, ultrafast and super-resolution ultrasound imaging were achieved using intravenous injection of microbubbles, the properties of which allowed haemodynamic quantification and imaging structures at 10mm under the cranium. Single echoes from individual microbubbles could be detected, allowing accurate quantification of blood flow speeds at an imaging rate of 1000 frames per second [112]. Altogether, technological improvements in ultrasound speed and resolution, as well as echosonography applications, hold enormous potential for parasitology in terms of studying changes in rheology, vascular permeability, tissue perfusion, and changes in the physiology of important structures such as the brain blood barrier.

Magnetic resonance imaging

Magnetic resonance imaging (MRI) is a non-invasive imaging technique uniquely suited to image deep inside tissue with high spatial resolution and without ionizing radiation. MRI is based on the magnetic properties of protons and neutrons within atomic nuclei of the body, particularly of hydrogen, as water is a major component of the human body. The spin of hydrogen nuclei can be measured as they show an uneven number of protons. Therefore, after placing the body inside the magnetic field of the MRI scanner, the spins start to process with the Lamour frequency and align with the magnetic field (in both directions, however slightly more in the field direction). Upon application of a radiofrequency (RF) pulse with exactly the same Lamour frequency, the nuclei can absorb energy and transition from lower to higher energy states (so called spin excitation). After the RF-pulse is switched off, the nuclei return to their equilibrium state. This process requires time and depends on the surrounding tissue (also known as relaxation time). During the relaxation process, a signal can be detected by RF coils in the scanner, which can be reconstructed by advanced imaging techniques to an image of the human body (reviewed by [114]). MRI offers extraordinary advantages, including high spatial resolution, and the opportunity of simultaneously extracting physiological, molecular, and anatomical information from the body. Conversely, its limitations include low sensitivity, long scanning time, and probe quantity required for imaging.

MRI has improved understanding of diseases in parasitology, by detecting pathological alterations e.g. in the brain caused by *Toxoplasma* [115] (**Figure 4a)**, *Trypanosoma brucei* [116] (**Figure**

4b), and *Plasmodium* [117] (**Figure 4c,** courtesy of Angelika Hoffmann). In this section we discuss the advances in the technique relevant to parasitology, in three specific aspects: MRI probes, multimodal mesoscopic imaging, and uses of functional MRI to address translational questions.

Contrast agents are exogenous compounds administered to improve the image contrast and detect pathological alterations more accurately. Significant efforts have been made to improve MRI by developing contrast agents for use as probes and sensors. These include gadolinium agents (Gd^{3+}) and derivatives including gadolinium hexanedione [118], gadofluorine and liposomal-based gadolinium nanoparticles [119]. These contrast agents are e.g. used in the study of brain nerve barrier permeability [120], blood vessel remodelling [121], or cellular uptake. Other agents include manganese-based agents such as manganese chloride ($MnCl_2$) [122], manganese oxide (MnO) [123], and silica-coated particles, which allow detection of specific cell populations *in vivo* either on their own, or by combining with other contrast agents. Equally, paramagnetic iron oxide (SPIO) agents, perfluorocarbons (PFCs), and highly shifted proton MRI [124–126], have been particularly useful for sensitively tracking and visualizing cell homing *in vivo* [127–129]. Altogether, advances in MRI contrast agents and probes have allowed monitoring functions of cells, including enzymatic activity, gene expression, and death, as well as sensitive tracking of cell populations (reviewed in [130]).

Secondly, while the output of MRI is imaging of anatomical changes, functional MRI (fMRI) is based on allowing visualization of metabolic function by tissues. fMRI allows measurement of blood flow changes, or blood oxygen level fluctuations, providing a picture of oxygen consumption. It is based on the use of blood oxygen level dependent (BOLD)-contrast, based on increased or decreased concentrations of paramagnetic deoxyhaemoglobin associated with changes in neuronal activity. (reviewed in [131]). The use of this technique has been relatively scarce in parasitology, yet has potential for a wide number of parasites, which induce metabolic and/or functional changes in tissues. Similarly, the generation of MRI scanners such as the 9.4 T equipment [132], offers improved imaging resolution.

Further X-ray and gamma-ray-based non-invasive imaging methods

Other imaging methods which have relevant clinical translation potential include radiography, computed tomography, X-ray micro-CT, and radioisotope-based imaging such as single photon emission computed tomography (SPECT) and positron emission tomography (PET). Two categories of X-ray-based imaging are structural and functional imaging enabling studies of anatomical structures, and of changes in biological functions such as metabolism, blood

flow, and biochemical composition of tissues. Functional analysis of tissues and their composition using X-rays has seen progress with the use of exogenous contrast agents, and is based on the possible interactions between X-rays and matter (**Figure 5**). These include X-ray attenuation, X-ray fluorescence and X ray excited optical luminescence (reviewed by [133,134]). Equally non-invasive is imaging based on gamma-emission from radioisotope-labelled biomolecules within samples upon radioactive decay, namely PET and SPECT. In both methods, radioactive biomolecules synthesized from radio-nucleotides are administered, and following biological interactions in specific tissues, decay, resulting in the emission of gamma photons. These photons can be detected by PET and SPECT scanners and can be tomographically reconstructed to generate 3D images of functional tissue activity [135]. The use of radiography-based and nuclear-imaging-based methods has been relatively limited in parasitology, yet has potential for the study of host-pathogen interaction effects on organ functions, tissue composition and metabolic changes upon infection.

Concluding remarks and future perspectives

Altogether, multiple methods for *in vivo* imaging as stand-alone techniques have allowed improved resolution (e.g., advanced microscopy methods such as super-resolution now possible with IVM), decreased invasiveness (e.g., by the use of OAI), increased penetration depth allowing for imaging of organ regions previously impossible to observe *in vivo* (e.g., through the use of GRIN lenses for IVM), and functional imaging with high resolution (e.g., fMRI, MRI). Although many of these techniques have successfully reached the parasitology field, particularly IVM, advances in IVM methods, and other techniques altogether, have enormous potential and applicability, which still need to be explored. Equally relevant is the use of hybrid, multimodality systems, which could provide the opportunity to study different host-pathogen interactions *in vivo*.

Acknowledgements

We are grateful to Volker Heussler (IZB, University of Bern) for helpful advice and intellectual input on the techniques relevant to OPT, LSFM, and OAI, and training and discussions key to these methods, and IVM. We thank also the MIC at the University of Bern, for providing access and training in all relevant imaging methods hereby discussed. We thank Federica Moalli, Renzo Danuser (TKI, Bern); Emmanuel G. Reynaud (University College, Dublin) and Jessica Kehrer

(Centre for Infectious Diseases, Heidelberg University Hospital) for helpful input for OPT and LSFM techniques and discussions. We thank Robert Nuster (IAP, Bern) for experimental help during the establishment of OAI for experimental cerebral malaria imaging. We are grateful to Angelika Hoffmann (Department of Neuroradiology, Heidelberg University Hospital) for her helpful input on MRI techniques, for kindly providing Figure 3C (MRI of a *Plasmodium*-infected brain*),* and for carefully proofreading this manuscript's sections relevant to MRI. MDN is funded by EMBO fellowship ALTF 1048-2016, and by an EVIMalaR (242095 FP7) and RSHTM (000529) fellowships with Volker Heussler (IZB, Bern) related to OPT and OAI studies, as well as Swiss National Science Foundation fellowships 310030_159519 and 316030_145013 funding work carried out in his lab. FS and MF acknowledge the financial support of the Swiss National Science Foundation (No: 205320_179038/1). Work in the laboratory of FF is funded by a Human Frontier Science Program grant (RGY 0066) and the German Science Foundation (SFB 1129). We apologize to the many colleagues for not citing their work due to restrictions by the journal and the broad scope of the review.

References

1 Nacer, A. *et al.* (2014) Experimental Cerebral Malaria Pathogenesis—Hemodynamics at the Blood Brain Barrier. *PLoS Pathog.* 10, e1004528

2 Coles, J.A. *et al.* (2015) Intravital Imaging of a Massive Lymphocyte Response in the Cortical Dura of Mice after Peripheral Infection by Trypanosomes. *PLoS Negl. Trop. Dis.* 9, e0003714

3 Konradt, C. *et al.* (2016) Endothelial cells are a replicative niche for entry of Toxoplasma gondii to the central nervous system. *Nat. Microbiol.* 1, 16001

4 Estato, V. *et al.* (2018) The Neurotropic Parasite Toxoplasma gondii Induces Sustained Neuroinflammation with Microvascular Dysfunction in Infected Mice. *Am. J. Pathol.* DOI: https://doi.org/10.1016/j.ajpath.2018.07.007

5 Amino, R. *et al.* (2006) Quantitative imaging of Plasmodium transmission from mosquito to mammal. *Nat. Med.* 12, 220–4

6 Hopp, C.S. *et al.* (2015) Longitudinal analysis of Plasmodium sporozoite motility in the dermis reveals component of blood vessel recognition. *Elife* 4, e07789

7 Peters, N.C. *et al.* (2008) In vivo imaging reveals an essential role for neutrophils in leishmaniasis transmitted by sand flies. *Science (80-.).* 321, 970–974

8 de Moraes, L.V. *et al.* (2013) Intravital Placenta Imaging Reveals Microcirculatory Dynamics Impact on Sequestration and Phagocytosis of Plasmodium-Infected Erythrocytes. *PLoS Pathog.* 9, e1003154

9 Lima, F.A. *et al.* (2014) Intravital microscopy technique to study parasite

dynamics in the labyrinth layer of the mouse placenta. *Parasitol. Int.* 63, 254–259
10 Frevert, U. *et al.* (2014) Imaging Plasmodium Immunobiology in Liver, Brain, and Lung. *Parasitol. Int.* 63, 10.1016/j.parint.2013.09.013
11 Tavares J, Formaglio P, Thiberge S, Mordelet E, Van Rooijen N, Medvinsky A, Menard R, A.R. (2013) Role of host cell traversal by the malaria sporozoite during liver infection. *J Exp Med* 210, 905–915
12 Sturm, A. *et al.* (2006) Manipulation of Host Hepatocytes by the Malaria Parasite for Delivery into Liver Sinusoids. *Science (80-.).* 313, 1287–1290
13 Beattie L, Peltan A, Maroof A, Kirby A, Brown N, Coles M, Smith DF, K.P. (2010) Dynamic Imaging of Experimental Leishmania donovani-Induced Hepatic Granulomas Detects Kupffer Cell-Restricted Antigen Presentation to Antigen-Specific CD8+ T Cells. *PLOS Pathog.* 6, e1000805
14 Martin-Jaular, L. *et al.* (2011) Strain-specific spleen remodelling in Plasmodium yoelii infections in Balb/c mice facilitates adherence and spleen macrophage-clearance escape. *Cell. Microbiol.* 13, 109–122
15 De Niz, M. *et al.* (2016) The machinery underlying malaria parasite virulence is conserved between rodent and human malaria parasites. *Nat Commun* 7,
16 Lagerweij, T. *et al.* (2017) Optical clearing and fluorescence deep-tissue imaging for 3D quantitative analysis of the brain tumor microenvironment. *Angiogenesis* 20, 533–546
17 Schuh, C.D. *et al.* (2016) Long wavelength multiphoton excitation is advantageous for intravital kidney imaging. *Kidney Int.* 89, 712–719
18 Friedl, P. *et al.* (2007) Biological Second and Third Harmonic Generation Microscopy. *Curr. Protoc. Cell Biol.* 34, 4.15.1-4.15.21
19 Perillo, E.P. *et al.* (2016) Deep in vivo two-photon microscopy with a low cost custom built mode-locked 1060 nm fiber laser. *Biomed. Opt. Express* 7, 324–334
20 Michalet, X. *et al.* (2005) Quantum Dots for Live Cells, in Vivo Imaging, and Diagnostics. *Science* 307, 538–544
21 Zhao, J. *et al.* (2018) Recent developments in multimodality fluorescence imaging probes. *Acta Pharm. Sin. B* 8, 320–338
22 Nobis, M. *et al.* (2018) Molecular mobility and activity in an intravital imaging setting – implications for cancer progression and targeting. *J. Cell Sci.* 131, jcs206995
23 Radbruch, H. *et al.* (2015) Intravital FRET: Probing Cellular and Tissue Function in Vivo. *Int. J. Mol. Sci.* 16, 11713–11727
24 Komatsu, N. *et al.* (2011) Development of an optimized backbone of FRET biosensors for kinases and GTPases. *Mol. Biol. Cell* 22, 4647–4656
25 Hires, S.A. *et al.* (2008) Reporting neural activity with genetically encoded calcium indicators. *Brain Cell Biol.* 36, 69–86
26 Tretiakova, D.S. *et al.* (2018) Lateral stress profile and fluorescent lipid probes. FRET pair of probes that introduces minimal distortions into lipid packing. *Biochim. Biophys. Acta - Biomembr.* 1860, 2337–2347

27 Kinoshita, M. *et al.* (2017) Emphatic visualization of sphingomyelin-rich domains by inter-lipid FRET imaging using fluorescent sphingomyelins. *Sci. Rep.* 7, 16801
28 Dai, T. *et al.* (2018) Liposomes and lipid disks traverse the BBB and BBTB as intact forms as revealed by two-step Förster resonance energy transfer imaging. *Acta Pharm. Sin. B* 8, 261–271
29 Hirata, E. and Kiyokawa, E. (2016) Future Perspective of Single-Molecule FRET Biosensors and Intravital FRET Microscopy. *Biophys. J.* 111, 1103–1111
30 Welf, E.S. *et al.* (2016) Quantitative Multiscale Cell Imaging in Controlled 3D Microenvironments. *Dev. Cell* 36, 462–475
31 Woehler, A. (2013) Simultaneous Quantitative Live Cell Imaging of Multiple FRET-Based Biosensors. *PLoS One* 8, e61096
32 Erami, Z. *et al.* (2016) Intravital FRAP Imaging using an E-cadherin-GFP Mouse Reveals Disease- and Drug-Dependent Dynamic Regulation of Cell-Cell Junctions in Live Tissue. *Cell Rep.* 14, 152–167
33 Machado, M.J.C. and Mitchell, C.A. (2011) Temporal changes in microvessel leakiness during wound healing discriminated by in vivo fluorescence recovery after photobleaching. *J. Physiol.* 589, 4681–4696
34 de Grauw, C.J. *et al.* (1999) Imaging properties in two-photon excitation microscopy and effects of refractive-index mismatch in thick specimens. *Appl. Opt.* 38, 5995
35 Andresen, V. *et al.* (2012) High-Resolution Intravital Microscopy. *PLoS One* 7, e50915
36 Wegner, W. *et al.* (2017) In vivo mouse and live cell STED microscopy of neuronal actin plasticity using far-red emitting fluorescent proteins. *Sci. Rep.* 7, 11781
37 White, M.D. *et al.* (2018) In Vivo Imaging of Single Mammalian Cells in Development and Disease. *Trends Mol. Med.* 24, 278–293
38 Kim, J.K. *et al.* (2012) Fabrication and operation of GRIN probes for in vivo fluorescence cellular imaging of internal organs in small animals. *Nat. Protoc.* 7, 1456–1469
39 Barretto, R.P.J. *et al.* (2011) Time-lapse imaging of disease progression in deep brain areas using fluorescence microendoscopy. *Nat. Med.* 17, 223–229
40 Reismann, D. *et al.* (2017) Longitudinal intravital imaging of the femoral bone marrow reveals plasticity within marrow vasculature. *Nat. Commun.* 8, 2153
41 Ducourthial, G. *et al.* (2015) Development of a real-time flexible multiphoton microendoscope for label-free imaging in a live animal. *Sci. Rep.* 5, 18303
42 Rueckel, M. *et al.* (2006) Adaptive wavefront correction in two-photon microscopy using coherence-gated wavefront sensing. *Proc. Natl. Acad. Sci. U. S. A.* 103, 17137–17142
43 Lee, S. *et al.* (2014) Automated motion artifact removal for intravital microscopy, without a priori information. *Sci. Rep.* 4, 4507

44 Taylor, J.M. (2014) Optically gated beating-heart imaging. *Front. Physiol.* 5, 481
45 Warren, S.C. *et al.* (2018) Removing physiological motion from intravital and clinical functional imaging data. *Elife* 7, e35800
46 Ntziachristos, V. (2010) Going deeper than microscopy: the optical imaging frontier in biology. *Nat Meth* 7, 603–614
47 Hama, H. *et al.* (2015) ScaleS: an optical clearing palette for biological imaging. *Nat Neurosci* 18, 1518–1529
48 Tomer, R. *et al.* (2014) Advanced CLARITY for rapid and high-resolution imaging of intact tissues. *Nat. Protoc.* 9, 1682–1697
49 Richardson, D.S. and Lichtman, J.W. (2016) Clarifying Tissue Clearing. *Cell* 162, 246–257
50 Ertürk, A. *et al.* (2012) Three-dimensional imaging of solvent-cleared organs using 3DISCO. *Nat. Protoc.* 7, 1983–1995
51 Dodt, H.-U. *et al.* (2007) Ultramicroscopy: three-dimensional visualization of neuronal networks in the whole mouse brain. *Nat Meth* 4, 331–336
52 Becker, K. *et al.* (2012) Chemical Clearing and Dehydration of GFP Expressing Mouse Brains. *PLoS One* 7, e33916
53 Abe, J. *et al.* (2016) Light sheet fluorescence microscopy for in situ cell interaction analysis in mouse lymph nodes. *J. Immunol. Methods* 431, 1–10
54 Hama, H. *et al.* (2011) Scale: a chemical approach for fluorescence imaging and reconstruction of transparent mouse brain. *Nat Neurosci* 14, 1481–1488
55 Ke, M.-T. *et al.* (2013) SeeDB: a simple and morphology-preserving optical clearing agent for neuronal circuit reconstruction. *Nat Neurosci* 16, 1154–1161
56 Chung, K. *et al.* (2013) Structural and molecular interrogation of intact biological systems. *Nature* 497, 332–337
57 Poguzhelskaya, E. *et al.* (2014) Simplified method to perform CLARITY imaging. *Mol. Neurodegener.* 9, 19
58 Sharpe, J. *et al.* (2002) Optical Projection Tomography as a Tool for 3D Microscopy and Gene Expression Studies. *Science (80-.).* 296, 541 LP-545
59 Kak, A.C., Slaney, M. (1988) *Principles of Computerized Tomographic Imaging*, IEEE Press.
60 Huisken, J. *et al.* (2004) Optical Sectioning Deep Inside Live Embryos by Selective Plane Illumination Microscopy. *Science (80-.).* 305, 1007–1009
61 Pampaloni, F. *et al.* (2007) The third dimension bridges the gap between cell culture and live tissue. *Nat Rev Mol Cell Biol* 8, 839–845
62 Huisken, J. and Stainier, D.Y.R. (2007) Even fluorescence excitation by multidirectional selective plane illumination microscopy (mSPIM). *Opt. Lett.* 32, 2608–2610
63 Mayer, J., Robert-Moreno, A., Danuser, R., Stein, J.V., Sharpe J., Swoger, J. (2014) OPTiSPIM: integrating optical projection tomography in light sheet microscopy extends specimen characterization to nonfluorescent contrasts. *Opt. Lett.* 39, 1053–1056
64 Pitrone, P.G. *et al.* (2013) OpenSPIM: an open-access light-sheet microscopy

platform. *Nat Meth* 10, 598–599
65 Gualda, E.J. *et al.* (2013) OpenSpinMicroscopy: an open-source integrated microscopy platform. *Nat. Methods* 10, 599
66 Jakob, P.H. *et al.* (2016) A 3-D cell culture system to study epithelia functions using microcarriers. *Cytotechnology* 68, 1813–1825
67 Pampaloni, F. *et al.* (2014) Tissue-culture light sheet fluorescence microscopy (TC-LSFM) allows long-term imaging of three-dimensional cell cultures under controlled conditions. *Integr. Biol.* 6, 988–998
68 Pampaloni, F. *et al.* (2015) Live Spheroid Formation Recorded with Light Sheet-Based Fluorescence Microscopy. In *Advanced Fluorescence Microscopy: Methods and Protocols* (Verveer, J. P., ed), pp. 43–57, Springer New York
69 Pampaloni, F. *et al.* (2015) Light sheet-based fluorescence microscopy (LSFM) for the quantitative imaging of cells and tissues. *Cell Tissue Res.* 360, 129–141
70 Correia, T. *et al.* (2015) Accelerated Optical Projection Tomography Applied to In Vivo Imaging of Zebrafish. *PLoS One* 10, e0136213
71 Chen, L. *et al.* (2015) Mesoscopic in vivo 3-D tracking of sparse cell populations using angular multiplexed optical projection tomography. *Biomed. Opt. Express* 6, 1253–1261
72 Maizel, A. *et al.* (2011) High-resolution live imaging of plant growth in near physiological bright conditions using light sheet fluorescence microscopy. *Plant J.* 68, 377–385
73 Summerhurst, K. *et al.* (2008) 3D representation of Wnt and Frizzled gene expression patterns in the mouse embryo at embryonic day 11.5 (Ts19). *Gene Expr. Patterns* 8, 331–348
74 Alves, S. *et al.* (2016) Ultramicroscopy as a novel tool to unravel the tropism of AAV gene therapy vectors in the brain. *Sci. Rep.* 6, 28272
75 Dobosz, M. *et al.* (2014) Multispectral Fluorescence Ultramicroscopy: Three-Dimensional Visualization and Automatic Quantification of Tumor Morphology, Drug Penetration, and Antiangiogenic Treatment Response. *Neoplasia* 16, 1–13
76 McGurk, L. *et al.* (2007) Three-Dimensional Imaging of Drosophila melanogaster. *PLoS One* 2, e834
77 Jährling, N. *et al.* (2010) Three-Dimensional Reconstruction and Segmentation of Intact Drosophila by Ultramicroscopy. *Front. Syst. Neurosci.* 4, 1
78 Yang, B. *et al.* (2014) Single-Cell Phenotyping within Transparent Intact Tissue Through Whole-Body Clearing. *Cell* 158, 945–958
79 Schuster, S. *et al.* (2017) Developmental adaptations of trypanosome motility to the tsetse fly host environments unravel a multifaceted in vivo microswimmer system. *Elife* 6, e27656
80 Badr, C.E. (2014) Bioluminescence Imaging: Basics and Practical Limitations BT - Bioluminescent Imaging: Methods and Protocols. (Badr, C. E., ed), pp. 1–18, Humana Press

81 Avci, P. *et al.* (2017) In-vivo monitoring of infectious diseases in living animals using bioluminescence imaging. *Virulence* 9, 28–63
82 Siciliano, G. and Alano, P. (2015) Enlightening the malaria parasite life cycle: bioluminescent Plasmodium in fundamental and applied research. *Front. Microbiol.* 6, 391
83 Calvo-Alvarez, E. *et al.* (2018) A new chimeric triple reporter fusion protein as a tool for in vitro and in vivo multimodal imaging to monitor the development of African trypanosomes and Leishmania parasites. *Infect. Genet. Evol.* 63, 391–403
84 Costa, F.C. *et al.* (2018) Expanding the toolbox for Trypanosoma cruzi: A parasite line incorporating a bioluminescence-fluorescence dual reporter and streamlined CRISPR/Cas9 functionality for rapid in vivo localisation and phenotyping. *PLoS Negl. Trop. Dis.* 12, e0006388–e0006388
85 Azevedo, M.F. *et al.* (2014) Plasmodium falciparum transfected with ultra bright NanoLuc luciferase offers high sensitivity detection for the screening of growth and cellular trafficking inhibitors. *PLoS One* 9, e112571–e112571
86 De Niz, M. *et al.* (2016) An ultrasensitive NanoLuc-based luminescence system for monitoring Plasmodium berghei throughout its life cycle. *Malar. J.* 15, 1–24
87 Hall, M.P. *et al.* (2012) Engineered luciferase reporter from a deep sea shrimp utilizing a novel imidazopyrazinone substrate. *ACS Chem. Biol.* 7, 1848–1857
88 Chu, J. *et al.* (2016) A bright cyan-excitable orange fluorescent protein facilitates dual-emission microscopy and enhances bioluminescence imaging in vivo. *Nat. Biotechnol.* 34, 760–767
89 Yeh, H.-W. *et al.* (2017) Red-shifted luciferase-luciferin pairs for enhanced bioluminescence imaging. *Nat. Methods* 14, 971–974
90 Kuchimaru, T. *et al.* (2016) A luciferin analogue generating near-infrared bioluminescence achieves highly sensitive deep-tissue imaging. *Nat. Commun.* 7, 11856
91 Iwano, S. *et al.* (2018) Single-cell bioluminescence imaging of deep tissue in freely moving animals. *Science (80-.).* 359, 935 LP-939
92 De Niz, M. *et al.* (2015) In vivo and in vitro characterization of a Plasmodium liver stage-specific promoter. *PLoS One* 10, e0123473–e0123473
93 Cevenini, L. *et al.* (2014) Multicolor bioluminescence boosts malaria research: quantitative dual-color assay and single-cell imaging in Plasmodium falciparum parasites. *Anal. Chem.* 86, 8814–8821
94 Komatsu, N. *et al.* (2018) A platform of BRET-FRET hybrid biosensors for optogenetics, chemical screening, and in vivo imaging. *Sci. Rep.* 8, 8984
95 Niederhauser, J.J. *et al.* (2005) Combined ultrasound and optoacoustic system for real-time high-contrast vascular imaging in vivo. *IEEE Trans. Med. Imaging* 24, 436–440
96 Held, K.G. *et al.* (2016) Multiple irradiation sensing of the optical effective attenuation coefficient for spectral correction in handheld OA imaging. *Photoacoustics* 4, 70–80

97 Oraevsky, A.A. *et al.* Laser-based optoacoustic imaging in biological tissues.
98 Kruger, R.A. *et al.* (1995) Photoacoustic ultrasound (PAUS)--reconstruction tomography. *Med. Phys.*
99 Weber, J. *et al.* (2016) Contrast agents for molecular photoacoustic imaging. *Nat. Methods* 13, 639
100 Beard, P. Biomedical photoacoustic imaging. , *Interface Focus*, 1. Aug-(2011) , 602–631
101 Schwarz, M. *et al.* (2015) Implications of ultrasound frequency in optoacoustic mesoscopy of the skin. *IEEE Trans. Med. Imaging* 34, 672–677
102 Laufer, J. *et al.* (2009) Three-dimensional noninvasive imaging of the vasculature in the mouse brain using a high resolution photoacoustic scanner. *Appl. Opt.* 48, D299--D306
103 Yao, J. and Wang, L. V (2014) Sensitivity of photoacoustic microscopy. *Photoacoustics* 2, 87–101
104 Hu, S. *et al.* (2011) Second-generation optical-resolution photoacoustic microscopy with improved sensitivity and speed. *Opt. Lett.* 36, 1134–1136
105 Wang, X. *et al.* (2006) Noninvasive imaging of hemoglobin concentration and oxygenation in the rat brain using high-resolution photoacoustic tomography. *J. Biomed. Opt.* 11, 24015
106 Razansky, D. *et al.* (2011) Volumetric real-time multispectral optoacoustic tomography of biomarkers. *Nat. Protoc.* 6, 1121–1129
107 Buehler, A. *et al.* (2010) Video rate optoacoustic tomography of mouse kidney perfusion. *Opt. Lett.* 35, 2475–2477
108 Taruttis, A. *et al.* (2010) Real-time imaging of cardiovascular dynamics and circulating gold nanorods with multispectral optoacoustic tomography. *Opt. Express* 18, 19592
109 Mercep, E. *et al.* (2015) Whole-body live mouse imaging by hybrid reflection-mode ultrasound and optoacoustic tomography. *Opt. Lett.* 40, 4643–4646
110 Bruce, M. *et al.* (2017) Limitations and artifacts in shear-wave elastography of the liver. *Biomed. Eng. Lett.* 7, 81–89
111 Chong, W.K. *et al.* (2018) Imaging with ultrasound contrast agents: current status and future. *Abdom. Radiol.* 43, 762–772
112 Errico, C. *et al.* (2015) Ultrafast ultrasound localization microscopy for deep super-resolution vascular imaging. *Nature* 527, 499
113 Kogan, P. *et al.* (2010) Microbubbles in Imaging: Applications Beyond Ultrasound. *Bubble Sci. Eng. Technol.* 2, 3–8
114 Grover, V.P.B. *et al.* (2015) Magnetic Resonance Imaging: Principles and Techniques: Lessons for Clinicians. *J. Clin. Exp. Hepatol.* 5, 246–255
115 Parlog, A. *et al.* (2014) Chronic murine toxoplasmosis is defined by subtle changes in neuronal connectivity. *Dis. Model. Mech.* 7, 459–469
116 Rodgers, J. *et al.* (2011) Magnetic Resonance Imaging to Assess Blood–Brain Barrier Damage in Murine Trypanosomiasis. *Am. J. Trop. Med. Hyg.* 84, 344–350
117 Hoffmann A, Helluy X, Fischer M, Mueller AK, Heiland S, Pham M,

Bendszus M, P.J. (2017) In Vivo Tracking of Edema Development and Microvascular Pathology in a Model of Experimental Cerebral Malaria Using Magnetic Resonance Imaging. *J Vis Exp* 8,
118 Tseng, C.-L. *et al.* (2010) Gadolinium hexanedione nanoparticles for stem cell labeling and tracking via magnetic resonance imaging. *Biomaterials* 31, 5427–5435
119 Ghaghada, K.B. *et al.* (2009) New Dual Mode Gadolinium Nanoparticle Contrast Agent for Magnetic Resonance Imaging. *PLoS One* 4, e7628
120 Wessig, C. (2011) Detection of Blood-Nerve Barrier Permeability by Magnetic Resonance Imaging. *Blood-Brain Other Neural Barriers Rev. Protoc.* 686, 267–271
121 Zheng, J. *et al.* (2009) MRI-based biomechanical imaging: initial study on early plaque progression and vessel remodeling. *Magn. Reson. Imaging* 27, 1309–1318
122 Aoki, I. *et al.* (2006) Cell labeling for magnetic resonance imaging with the T1 agent manganese chloride. *NMR Biomed.* 19, 50–59
123 Gilad, A.A. *et al.* (2008) MR tracking of transplanted cells with "positive contrast" using manganese oxide nanoparticles. *Magn. Reson. Med.* 60, 1–7
124 Schmidt, R. *et al.* (2014) Highly Shifted Proton MR Imaging: Cell Tracking by Using Direct Detection of Paramagnetic Compounds. *Radiology* 272, 785–795
125 Germuska, M. and Bulte, D.P. (2014) MRI measurement of oxygen extraction fraction, mean vessel size and cerebral blood volume using serial hyperoxia and hypercapnia. *Neuroimage* 92, 132–142
126 Bulte, J.W.M. (2014) Science to Practice: Highly Shifted Proton MR imaging—A Shift toward Better Cell Tracking? *Radiology* 272, 615–617
127 Cromer Berman, S.M. *et al.* (2011) Tracking stem cells using magnetic nanoparticles. *Wiley Interdiscip. Rev. Nanomedicine Nanobiotechnology* 3, 343–355
128 Partlow, K.C. *et al.* (2007) 19F magnetic resonance imaging for stem/progenitor cell tracking with multiple unique perfluorocarbon nanobeacons. *FASEB J.* 21, 1647–1654
129 Kadayakkara, D.K. *et al.* (2014) (19)F Spin-lattice Relaxation of Perfluoropolyethers: Dependence on Temperature and Magnetic Field Strength (7.0-14.1T). *J. Magn. Reson.* 0, 18–22
130 Srivastava, A.K. *et al.* (2015) Advances in using MRI probes and sensors for in vivo cell tracking as applied to regenerative medicine. *Dis. Model. Mech.* 8, 323–336
131 Pike, G.B. (2012) Quantitative functional MRI: Concepts, issues and future challenges. *Neuroimage* 62, 1234–1240
132 Felder, J. *et al.* (2017) 9.4 T small animal MRI using clinical components for direct translational studies. *J. Transl. Med.* 15, 264
133 Baird, E. and Taylor, G. (2017) X-ray micro computed-tomography. *Curr. Biol.* 27, R289–R291
134 Chen, H. *et al.* (2013) Monitoring pH-triggered drug release from radioluminescent nanocapsules with X-ray excited optical luminescence.

ACS Nano 7, 1178–1187
135 Rahmim A, Z.H. (2008) PET versus SPECT: strengths, limitations and challenges. *Nucl. Med. Commun.* 29, 193–207

Imaging method	Resolution	Penetration depth (max)	Advantages	Potentail parasitology applications in *in vivo* imaging
Electron microscopy (and combinations with fluorescence microscopy)	2–5 nm	1 μm (TEM)	Visualizes not just the fluorophore. Can now be combined with fluorescence microscopy (correlative light and electron microscopy: CLEM) and intravital imaging.	Observation of ultrastructural details of host–pathogen interactions, cells, and infection-related changes.
STED	20 nm (lateral)	100–200 μm	Enables fluorescent imaging at a nano-scale resolution.	Observation of highly resolved structures and host–parasite interactions at subcellular resolution.
IVM: Advanced fluorescence microscopy – FRET	2–10 nm	100–200 μm	Enables quantification of protein–protein interactions *in vivo*.	Monitor enzyme activities, ion changes, host–pathogen interactions, lipid changes, mechanical stress, and molecule quantifications.
IVM: Advanced fluorescence microscopy – FRAP	2–10 nm	100–200 μm	Enables quantification of lateral diffusion dynamics.	Monitor host–pathogen interactions at the subcellular level within cells harbouring intracellular parasites, for example, organelle hijacking, nutrient acquisition.
IVM: Advanced fluorescence microscopy – FLIP	200 nm	100–200 μm	Enables quantification of membrane dynamics.	Monitor host–pathogen interactions at the subcellular level, for example, intracellular parasite membrane fusion and organelle segregation during replication.
IVM: Confocal imaging	200 nm	100–200 μm	Compromise between high resolution and fast acquisition rates *in vivo*.	Monitor host–pathogen interactions at subcellular and cellular levels.
IVM: Multiphoton microscopy	400 nm	500–800 μm	The highest advantage over other methods is high penetration depth. Low background autofluorescence.	Monitoring parasite dynamics in deep organ structures.
IVM: Spinning-disc microscopy	200 nm	100–200 μm	Fast image acquisition speed *in vivo*.	Monitoring dynamics of host–pathogen interactions, membrane dynamics, tissue changes, vasculature at near real time.
OPT	20 μm	cm in cleared samples	3D reconstruction of large, optically cleared samples.	Visualizing parasite and tissue distribution, vascular changes, and systemic changes at whole-tissue and even whole-animal level.
SPIM	200–500 nm	cm in cleared samples	3D reconstruction of large, optically cleared samples. Little phototoxicity in live imaging.	Visualizing parasite and tissue distribution, vascular changes, and systemic changes at whole-tissue and even whole-animal level.
OAI	Sub-100 μm in deep tissues	cm	Images noninvasively optical absorption contrast over a wide range of spatial scales at high speed. Able to image structures and function.	Noninvasive imaging of effects of parasite presence in tissues. Visualization of vascular and metabolic changes in various organs longitudinally.
MRI	100–500 μm	Full body	Noninvasive imaging, applicable to clinics. Provides detailed information on tissue architecture, morphology, pathology.	Can be applied to organs ranging from deep organs to skin, to study parasite effects at tissue level. Functional MRI can be used to study function in tissues affected by parasite presence.
Radiography	cm	Full body	Noninvasive imaging. Provides detailed information on tissue architecture.	Applicable to study tissue diffraction properties upon infection with different parasites.
Ultrasound	Sub-100 μm in deep tissues	Full body	Noninvasive imaging, applicable to clinics. Provides detailed information on tissue architecture, morphology, pathology.	Can be applied to organs to study parasite effects at tissue level, including metabolic changes.
CT	mm	Full body	Noninvasive 3D imaging, applicable to clinics.	Can be applied to organs to study parasite effects at tissue level.
Bioluminescence imaging	cm	Several cm	Enables whole-body imaging in a high-throughput manner. Consistent with 3Rs on animal usage.	Visualizing luminescent parasite distribution. Potential to perform BRET *in vivo* has not been explored.
PET	mm	Full body	Allows observation of metabolic processes within the body, as well as parameters such as blood flow, metabolism, and neurotransmitters.	Observation of the effects of parasitic infections on host metabolism, blood flow perturbations, or neurotransmission at a whole-body level.
SPECT	Several mm	Full body	Allows observation of metabolic processes within the body, as well as parameters such as blood flow, metabolism, and neurotransmitters.	Observation of the effects of parasitic infections on host metabolism, blood flow perturbations, or neurotransmission at a whole-body level.

Table 1 Imaging scales and current/potential applications in parasitology.

	Organs/ pathogen	Central/peripheral nervous system	Skin	Lungs	Heart	Stomach/ pancreas	Liver	Spleen	Intestines	Kidneys/ bladder	Lymph nodes	Bone marrow	Adipose tissue	Placenta
Vector-borne	*Plasmodium* spp.	[1]	[5,6]	[13]	–	–	[14,15]	[19,20]	–	–	[23]	[25]	[20]	[26,27]
	Trypanosoma brucei	[2]	[7,8]	–	–	–	–	–	–	–	–	–	–	–
	Trypanosoma cruzi	–	[10,11]	–	–	–	–	–	–	–	–	–	–	–
	Onchocerca	–	–	–	–	–	–	–	–	–	–	–	–	–
	Leishmania	–	[9]	–	–	–	[16]	–	–	–	[24]	–	–	–
	Wuchereria/Brugia	–	–	–	–	–	–	–	–	–	–	–	–	–
	Schistosoma	–	[12]	–	–	–	[17]	–	–	–	–	–	–	–
	Theileria	–	–	–	–	–	–	–	–	–	–	–	–	–
	Babesia	–	–	–	–	–	–	–	–	–	–	–	–	–
Food/water/soil-borne	*Toxoplasma*	[3,4]	–	–	–	–	–	–	[21,22]	–	–	–	–	–
	Entamoeba	–	–	–	–	–	[18]	–	–	–	–	–	–	–
	Echinococcus	–	–	–	–	–	–	–	–	–	–	–	–	–
	Ascaris	–	–	–	–	–	–	–	–	–	–	–	–	–
	Ancylostoma	–	–	–	–	–	–	–	–	–	–	–	–	–
	Necator	–	–	–	–	–	–	–	–	–	–	–	–	–
	Strongyloides	–	–	–	–	–	–	–	–	–	–	–	–	–
	Paragonimus	–	–	–	–	–	–	–	–	–	–	–	–	–
	Giardia	–	–	–	–	–	–	–	–	–	–	–	–	–
	Cryptosporidium	–	–	–	–	–	–	–	–	–	–	–	–	–

Table 2 Key examples of organs and parasites by IVM. Table includes key examples for each parasite and organ rather than an exhaustive coverage. Green – IVM exists; yellow – organ relevant, but IVM never done; Grey – IVM not done.

Clearing method	Rationale	Advantages	Limitations	Refs
BABB (Murray's clear; Benzyl alcohol: benzyl benzoate)	Benzyl alcohol and benzyl-benzoate.	Quick tissue clearance. Successful for clearing connective tissues.	Strong quenching of fluorescence. Solutions used are toxic.	[62]
3DISCO (3D imaging of solvent-cleared organs)	Tetrahydrofluorane, dichloromethane, and dibenzyl ether.	Successfully preserves fluorescence in tissues (brain) while enabling adequate tissue clearance.	Fluorescence quenching in some tissues. Clearance not very fast.	[63]
iDISCO (immunolabelling-enabled 3D imaging of solvent-cleared organs)	Uses dibenzylether.	Enables deep antibody diffusion in large organs. Compatible with use of Alexa Fluor dyes: does not require immediate imaging as there is no diffusion over time.	Minor.	[64]
PACT (passive clarity technique), PARS and RIMS	Passive tissue clearing and immunostaining of intact organs. Uses acrylamide, bis-acrylamide, and SDS (sodium dodecyl sulfate).	Preserves fluorescence successfully. Low maintenance procedure.	Long incubation time required. Can cause aberrations in tissue morphology.	[60]
CUBIC (clear unobstructed brain-imaging cocktails and computational analysis)	Urea, N,N,N′,N′-tetrakis (2-hydroxypropyl)ethylenediamine, Triton X-100, sucrose, and 2,2′,2″-nitrilotriethanol.	Relatively fast procedure, preserves tissue morphology and fluorescence intensity. Whole-body clearance is possible via trans-cardial perfusion with reagents.	Minor.	[65,66]
RTF	Rapid clearing method based on triethanolamine and formamide.	Can render tissues transparent within hours. Is user friendly. Preserves fluorescence signal (including GFP) and tissue structure.	Minor. Not yet validated in multiple organs.	[67]
TDE (tetrachlorodiphenylethane)	Based on 2,2′-thiodiethanol, a glycol derivative often used as mounting medium.	Reported use in brain with successful clearance and fluorescence preservation.	In high concentrations, TDE quenches fluorescence, and affects cell shape.	[68,69]
Spalteholz	Benzyl alcohol, benzyl benzoate and methylsalicylate isosafrole.	Quick tissue clearance. Successful for clearing connective tissues.	Strong quenching of fluorescence. Solutions used are toxic.	[70]
SWITCH (system-wide control of interaction time and kinetic of chemicals)	SDS and custom refractive index-matching solution. Requires glutaraldehyde and thermal delipidation, followed by refractive index-matching. Increases hybrid porosity, facilitating diffusion for labelling.	Very strong and fast clearing. Allows clearing while preserving fluorescence and antigenicity across the tissue. Buffer allows chemical reactions between exogenous and endogenous molecules. Suitable for multiplexed proteomic imaging.	Can introduce colouration artefacts.	[71]
Sca*l*eA2/U2	Urea, glycerol, and Triton X-100	Glycerol counter-balances urea-induced tissue expansion. Allows targeting lipophilic tissue regions.	Slow clearance rates. Aberrations can be introduced due to reagents used, including tissue fragility and volume enlargement of specimens. Not good in heavily myelinated tissues.	[72]
Sca*l*eS	Optimized Sca*l*e protocol. Sorbitol-based.	Preserves tissue morphology and fluorescence. Sorbitol is effective at clearing tissues otherwise difficult to clear. Allows imaging at high resolution and significant depth.	Not all tissues are successfully cleared using this method. As Sca*l*e A2/U2, not so successful in heavily myelinated tissues.	[59]
FRUIT	SeeDB-derived method that uses D (–)-fructose and urea.	Water-soluble method has additive clearance effects. Allows arterial perfusion for enhanced clearance. Compatible with yellow fluorescence	Minor. Usefulness not yet reported in multiple tissue types.	[73]
		proteins. Compatible with use of lipophilic tracers.		
Clear^{T}	Based on formamide.	Since it does not use detergents or solvents, allows the use of lipophilic dyes and fluorescent tracers. Clearing speed of some tissues.	The main component is toxic. Insufficient tissue transparency for full volume imaging. Quenches fluorescence, especially GFP.	[74]
Clear^{T2}	Based on formamide and polyethylene glycol (PEG).	Allows the use of lipophilic dyes and fluorescent tracers. Clearing speed of some tissues. PEG stabilizes protein conformation, thus inhibits GFP quenching.	Insufficient tissue transparency for full-volume imaging.	[75]
SeeDB (See Deep Brain)	Combination of fructose and α-thioglycerol.	Fast clearing with optimal preservation of tissue integrity and fluorescence signal. Allows large-scale imaging.	Viscosity of saturated fructose is very high. Difficult to permeate organs. Arterial perfusion not possible.	[76]
CLARITY (clear lipid-exchanged acrylamide hybridized rigid imaging compatible tissue hydrogel)	Bioelectrochemical clearing technique. Builds an acrylamide-based hydrogel hybrid from intact tissues. Uses electrophoresis, acrylamide, bis-acrylamide, and SDS.	Preserves fluorescence successfully.	Electrophoresis base can be challenging to implement. Can damage tissues or introduce artefacts.	[77,78]
MAP (magnified analysis of the proteome)	Based on CLARITY method, uses denser gel to provide the tissue with more stability.	Allows preservation of the tissue integrity while allowing successful tissue clearance. Allows linear tissue expansion, and therefore highly resolved imaging. Allows multiple rounds of immune-labelling.	Minor.	[79]

Table 3 Tissue clearance methods for SPIM and OPT.

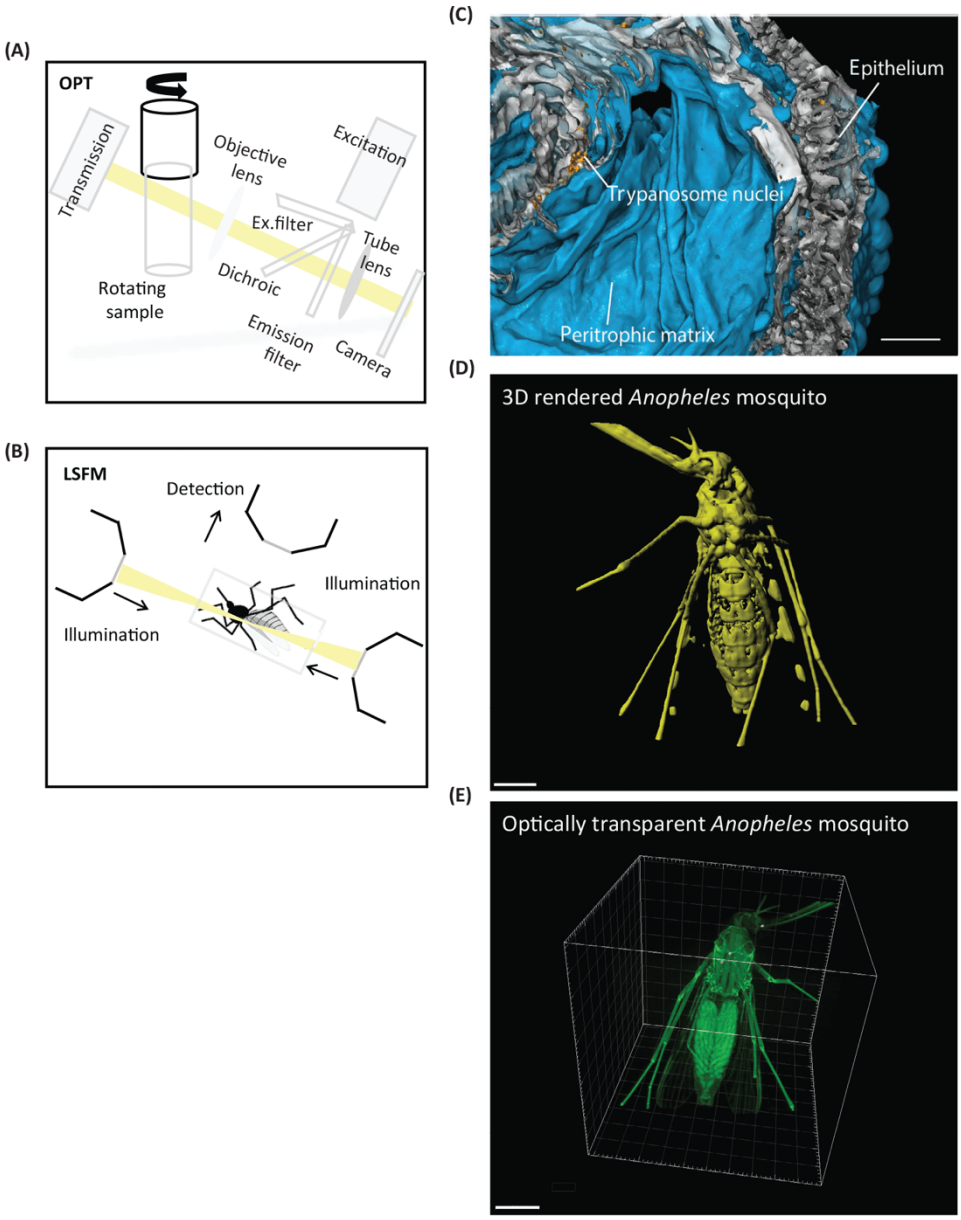

Figure 1 Optical projection tomography and selective plane illumination microscopy

(A) Principle of OPT. The optically cleared specimen is embedded in agarose, attached to a metallic cylinder within a rotating stage, and suspended in an index-matching liquid to reduce scattering and heterogeneities of refractive index throughout the specimen. When the specimen is rotated to a series of angular positions, images are captured at each orientation. The setup is aligned to ensure that the axis of rotation is perpendicular to the optical axis, so that straight line projections going through the sample can be generated, and collected by pixels on the CCD of the camera. **(B)** Principle of LSFM. The optically cleared sample is embedded in agarose, and suspended within a sample holder inside an index-matching liquid. A thin (nm – um) slice of the sample is illuminated perpendicularly to the direction of observation. Scanning is performed using a plane of light, which allows very fast image acquisition. **(C)** Surface rendering model of isolated infected fly guts. The intestinal tissue is visualised by autofluorescence (grey). The PM is stained

with rhodamine-labelled WGA (cyan) and the trypanosome nucleus with a GFP-reporter (yellow). **(D)** 3D reconstruction and rendering of a female *Anopheles* mosquito clearly showing abdominal segments, thorax and head features. **(E)** 3D reconstruction and clear view of all body cavities of an optically cleared *Anopheles* mosquito.

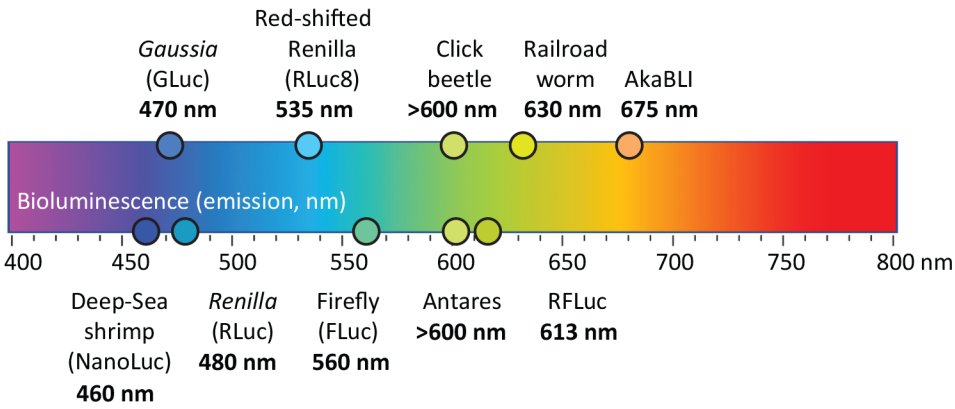

Figure 2 Bioluminescence imaging probes

Bioluminescence probes commonly used in *in vivo* imaging include Gaussia luciferase, NanoLuc, Renilla luciferase, click beetle luciferase (and its red- and green-shifted forms), red-shifted firefly luciferases, railroad worm luciferases, and novel probes with bright luminescence to image deep into tissues such as AkaBLI and Antares/Antares2. Isolated from different organisms, these probes have a varied range of molecular weights and maximum peak of emission wavelengths as schematically illustrated here, allowing for dual luminescence systems to be used.

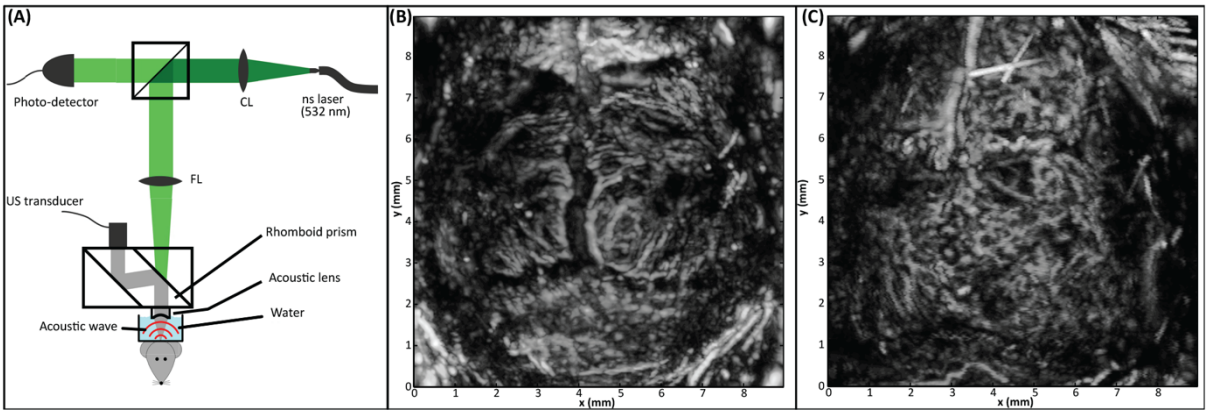

Figure 3 Optoacoustic microscopy setup and imaging of the brain

(A) Optoacoustic (OA) microscopy setup (acoustical resolution). The laser illumination induces thermo-elastic pressure waves in the sample and triggers signal acquisition (photodetector). The generated pressure wave (red) is collected by the acoustic lens and directed to the US transducer. **(B)** OA microscopic image of the brain of a healthy mouse shows clearly distinguishable hemispheres **(C)** the same image of a mouse infected with *Plasmodium* (5 days after infection) shows chaotic structure of the vasculature.

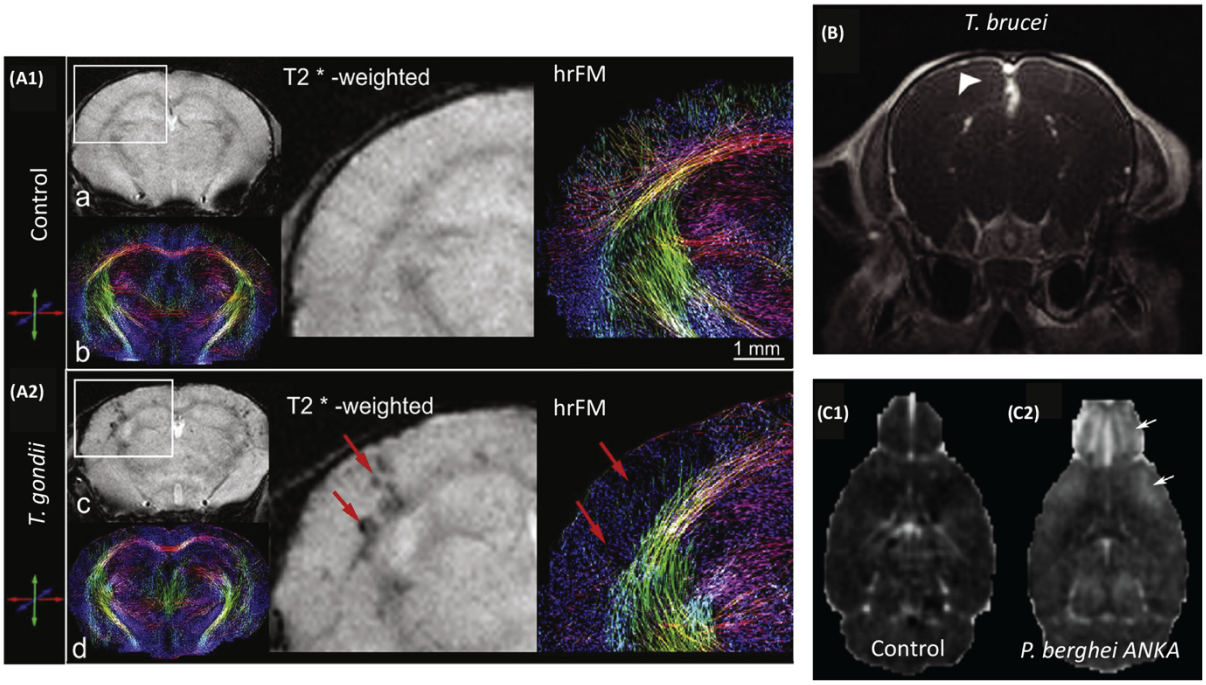

Figure 4 Magnetic Resonance Imaging of the brain

(A) T2*-weighted images and high resolution fiber maps of (A1) uninfected and (A2) *T. gondii* infected mouse brains. Arrows in infected brains show injuries in the somato-sensory cortex (T2*-weighted images), and affected fiber density and cortical connectivity pattern (hrFM images). **(B)** MRI scan of a mouse at 28 days post-infection with *T. brucei*, following administration of contrast. Arrow shows meningeal enhancement of the hind-most section of the brain. **(C)** T1 subtraction maps to illustrate blood-brain barrier (BBB) disruption with rostral predominance in a *Plasmodium*-infected mouse (C1) compared to a mouse not displaying BBB disruption (C2) (courtesy of Angelika Hoffmann).

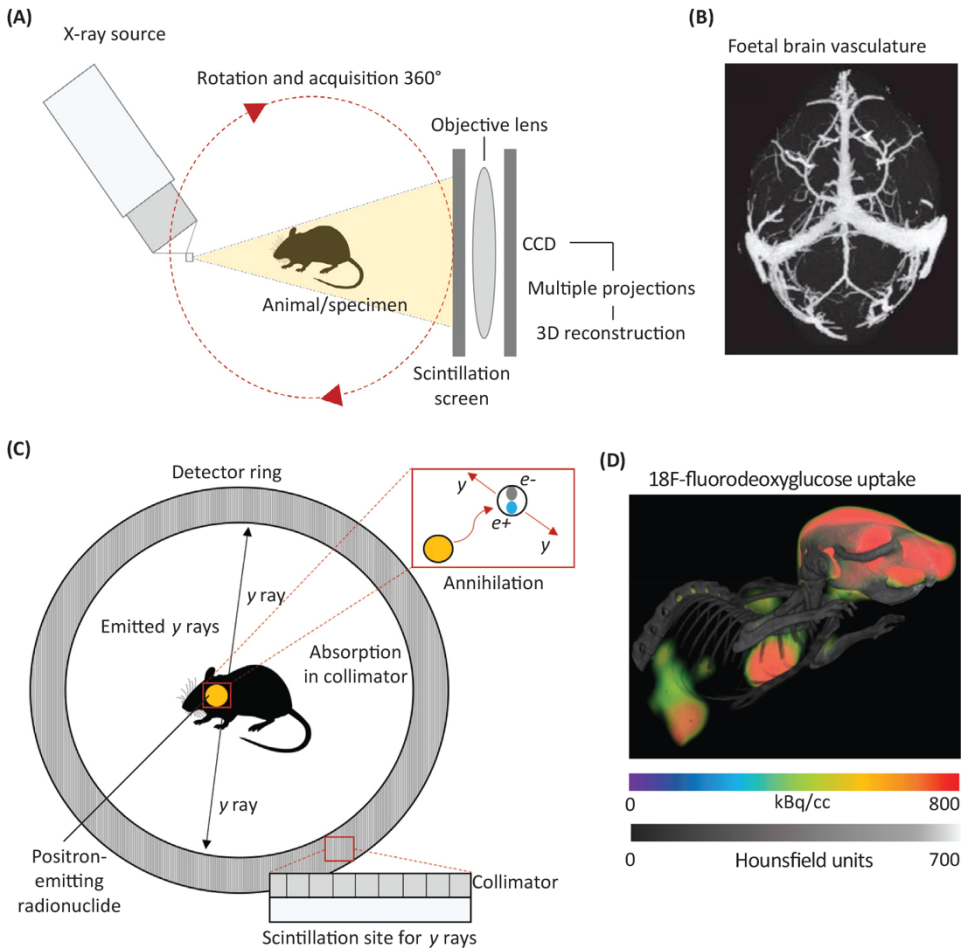

Figure 5. X-Ray-Based and Positron Emission Tomography (PET)-Based Imaging. (A) Principal components of a microcomputer tomography scanner include an X-ray source that produces X-rays which travel through the sample and are collected on the other side by an X-ray detector (scintillation screen, lens, and charge-coupled device camera). Rotation of the X-ray source and detector allows acquisition over 360_, allowing the generation of a series of projection images. These images can be processed to produce a 3D image of the specimen. **(B)** Maximum-intensity projection from an X-ray micro-computed tomography (micro-CT) study of the brainvasculature of foetuses from malaria-infected rodent mothers. The brain vasculature shown is that of a foetus from an uninfected mouse. Figure adapted from [154]. **(C)** Radioactive tracers are injected into the mouse and will emit positrons by radioactive decay. Upon decay, positrons are released from the nucleus of the radionuclide and annihilate with electrons in the tissue, releasing gamma-photons that can be detected within a coincidence detector ring (composed of a collimator and scintillation crystals). This allows mapping the anatomical localization of the tracer. **(D)** 3D reconstruction of a mouse imaged by PET-CT in a study investigating glucose uptake during the dark phase of a 24 h light–dark cycle. (18)F-fluorodeoxyglucose (FDG) was used as a tracer, and shows highest accumulation in the brain, heart, and bladder, followed by the kidneys and brown adipose tissue. Scale bars represent CT intensity (grey scale), and FDG uptake (colour

scale, radioactivity per tissue volume). Figure adapted from [155].